Journal of Experimental Nanoscience
Publication details, including instructions for authors and subscription information:
http://www.informaworld.com/smpp/title~content=t716100757

Analysis of the nanodiamond particle fabricated by detonation

Q. Zou[a]; M. Z. Wang[a]; Y. G. Li[a]
[a] State Key Laboratory of Metastable Materials Science and Technology, Yanshan University, Qinhuangdao 066004, Hebei, P.R. China

Online publication date: 07 July 2010

To cite this Article Zou, Q. , Wang, M. Z. and Li, Y. G.(2010) 'Analysis of the nanodiamond particle fabricated by detonation', Journal of Experimental Nanoscience, 5: 4, 319 — 328
To link to this Article: DOI: 10.1080/17458080903531021
URL: http://dx.doi.org/10.1080/17458080903531021

Journal of Experimental Nanoscience
Vol. 5, No. 4, August 2010, 319–328

Taylor & Francis
Taylor & Francis Group

Analysis of the nanodiamond particle fabricated by detonation

Q. Zou, M.Z. Wang* and Y.G. Li

State Key Laboratory of Metastable Materials Science and Technology, Yanshan University, Qinhuangdao 066004, Hebei, P.R. China

(*Received 5 June 2009; final version received 4 December 2009*)

In order to comprehensively analyse the structures and the surface states of the nanodiamond particles fabricated by detonation, various apparatus were used to investigate the nanodiamond powder including a high-resolution transmission electron microscope, an energy diffraction spectrometer, an X-ray diffractometer, a Raman spectrometer, a Fourier transform infrared spectrometer and differential scanning calorimeter. The grain size of the nanodiamond particles was in the range of 2–12 nm. However, the average grain size of the nanodiamond was approximately 5 nm. Moreover, the shapes of the nanodiamond particles were spherical or elliptical. The nanodiamond as fabricated was very pure, containing almost only the element of carbon. The contents of the impure element including O, Al and S were very small, which came from the synthesis and purification processes when fabricating the nanodiamond. The surfaces of the nanodiamond particles absorbed many functional groups, such as hydroxy, carbonyl, carboxyl and ether-based resin. The initial oxidation temperature of the nanodiamond powder in the air was about 520°C, which was lower than that of the bulk diamond. However, the oxidation temperature of the nanographite existing in the nanodiamond powder was about 228°C. The graphitisation temperature of the nanodiamond powder in the Ar gas was approximately 1305°C.

Keywords: nanodiamond; structure; surface state; analysis

1. Introduction

The nanodiamond, fabricated by detonation [1–4], not only has all the characteristics of bulk diamond but also has all the characteristics of powders, including large surface area, good chemical activity, large entropy and more structural defects [5]. These make the nanodiamond to have special optical, thermal and magnetic properties. It has been extensively researched and applied in the fields of composite coating [6,7], grinding [8], polishing [9], lubrication, photographic materials, high-strength resin and rubber, nanocomposite [10–12], seeds, drugs [13], thin film for nanotechnology [14,15] and so on.

*Corresponding author. Email: zq@ysu.edu.cn

ISSN 1745–8080 print/ISSN 1745–8099 online

DOI: 10.1080/17458080903531021
http://www.informaworld.com

As is well known, it is very difficult to carry out on-line analysis of the explosion and decomposition during the process of fabricating the nanodiamond because the chemical reaction process of the detonator explosion is extremely fast and very complex. In this work, a high-resolution transmission electron microscope (HRTEM), an energy diffraction spectrometer (EDS), an X-ray diffractometer (XRD), a Raman spectrometer (Raman), a Fourier transform infrared spectrometer (FTIR) and differential scanning calorimeter (DSC) were used to investigate comprehensively the structure and the surface states of the nanodiamond fabricated by the method of detonation.

2. Experiments

The nanodiamond used in this work was bought from Shenzhen Telecom Science & Technology Company (China). The nanodiamond was fabricated by the explosion of a detonator. The detonators of TNT/RDX were mixed in the mass ratio of 50/50. The protective gas was CO_2 during the process of explosion. The so-called 'carbon nanoaggregates' was prepared by detonation in a high-strength container using water cooling medium. The product of 'black powder' was collected after the detonation. A 100 sieve was used to remove the metal wire, plastic sheets and other pieces of impurities. Hydrochloric acid was then used to remove the impurities, such as metals and oxides caused by the container wall. Finally, deionised water was used to wash close to neutral pH and carbon nanoaggregates could be obtained after drying at the temperature of 80°C in vacuum. An acid oxidation liquid was used to deal with the carbon nanoaggregates at a high temperature to get nanodiamond [16–20].

A HRTEM (JEM-2010, Japan) was used to observe the microstructure of the nanodiamond. The accelerating voltage was 200 kV. The lattice resolution was 0.14 nm. The spot resolution was 0.23 nm. An EDS (Kevex-Sigmal Level 4, China) was used to determine the elements of the nanodiamond. The range of analysis was from B to U. The resolution was Mn 129 eV and F 65 eV. In this research, the nanodiamond was suppressed into thin slices for the EDS measurement. An XRD (D/MAX-rB, Japan) was used to determine qualitatively and quantitatively the phases, the lattice parameters and the grain size and to analyse the distortion. Copper target (Ka line) and graphite monochromator combined PHA monochrome. The accelerating voltage was 40 kV, the tube current was 100 mA, the maximum power was 12 kW, the wavelength was $\lambda_0 = 0.15406$ nm, the goniometer accuracy was $\pm 0.001°$, the scanning angle was from 10° to 100°. A Raman/FTIR spectrometer (E55+FRA 106/EQUINO × 55, Germany) was used to calibrate the structures of the nanodiamond and the molecules adsorbed on the surfaces of the nanodiamond. The wavelength range was from 10,000 to 370 cm^{-1}. The resolution was better than 0.5 cm^{-1}. The wavenumber accuracy was better than 0.01 cm^{-1}. The transmittance accuracy was better than 0.1% T. The signal-to-noise ratio was higher than 3600 : 1 (peak–peak). The resolution of the spectral range was from 2200 to 2100 cm^{-1}. A DSC (STA 449C, Germany) was used for the measurement of the initial oxidation temperature of the nanodiamond in the air and the graphitisation of the nanodiamond in the inert gas. The measuring temperature range was from −120°C to 1650°C. The specific heat measurement temperature range was from the room temperature to 1400°C. The specific heat range measured was from 0.1 to 5.0 $J\,g^{-1}K^{-1}$. The accuracy of

the specific heat measurement was approximately 5%. The repeatability of baseline was about 1 μV. The accuracy of temperature was less than 1 K. The maximum vacuum was 10^{-4} MPa.

3. Results and discussion

Figure 1 shows the HRTEM image and the diffraction ring of the nanodiamond. Figure 1(a) is a low-magnification HRTEM image of the nanodiamond. From this image, we can see that the nanodiamond particles were basically spherical or elliptical. The smallest particle size was about 2 nm and the largest particle size was about 12 nm. Through statistical analysis, the average size of the nanodiamond particles was determined to be 5 nm. Figure 1(b) is a high-magnification HRTEM image of the nanodiamond. From the HRTEM image, it also can be observed that there were twin crystals and stacking faults, such as defects, in the nanodiamond particles. The (1 1 1) surface spacing of the nanodiamond was approximately 0.2 nm. Figure 1(c) is the diffraction ring of the nanodiamond. Its diffraction was the polycrystalline ring, which demonstrated that

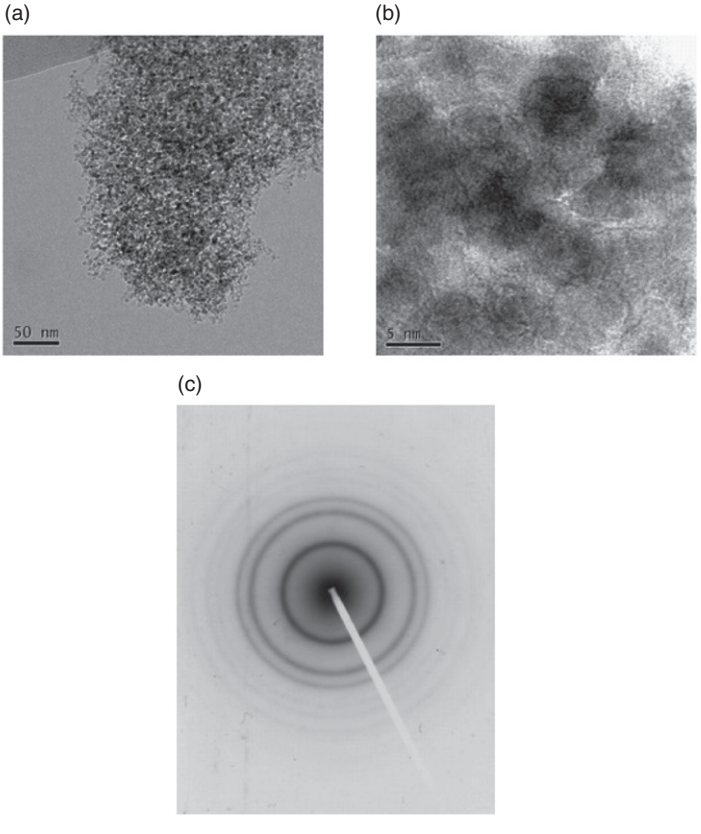

Figure 1. HRTEM image of the nanodiamond: (a) low-magnification; (b) high-magnification; (c) diffraction ring.

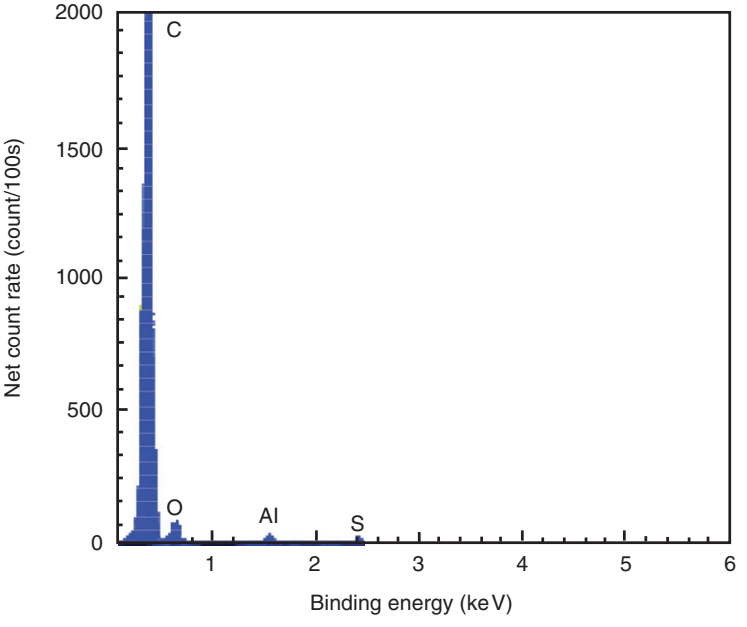

Figure 2. EDS spectrum of the nanodiamond.

the nanodiamond particles were very small. The corresponding electron diffraction also confirmed the diamond crystal structure.

Figure 2 shows the EDS spectrum of the nanodiamond. From this result, we know that the sample was very pure. Except for C, O, Al and S elements, there were no other elements. Moreover, the content of O, Al and S was relatively low. The oxygen was introduced from the environment. The Al came from the detonator. The element S was introduced by post-processing while preparing the nanodiamond.

Figure 3 shows the XRD pattern of the nanodiamond. As shown in Figure 3, the diffraction pattern of the nanodiamond showed three broader peaks at $2\theta = 43.8^\circ$, 75.2° and 91.1° corresponding to the (1 1 1), (2 2 0) and (3 1 1) cubic diamond planes, which demonstrated that the nanodiamond crystal was cubic. The peak at 20°–30° corresponded to the (0 0 2) crystal graphite plane. The diffraction peaks were obviously broadened owing to the very small size of the nanodiamond crystal, strains and defects. There was stronger background in the lower angle region ($<15^\circ$) for the whole spectrum, suggesting that there was a certain amorphous material existing in the nanodiamond powder. The XRD result agreed with the EDS result as shown in Figure 2.

The Raman spectrum of the nanodiamond is shown in Figure 4. For the macro-sized graphite and the bulk diamond crystals, there are very sharp peak features usually in the vicinity of 1332 and 1581 cm^{-1} observed, corresponding to the diamond and graphite, respectively. In the Raman spectrum of the nanodiamond, except the two wide Raman peaks in the vicinity of 1329 and 1580 cm^{-1}, there were no other Raman peaks.

Figure 5 shows the FTIR spectrum of the nanodiamond. From this spectrum, we can see that the peak at 3427 cm^{-1} was assigned to the $-OH$ stretching vibration and the peak

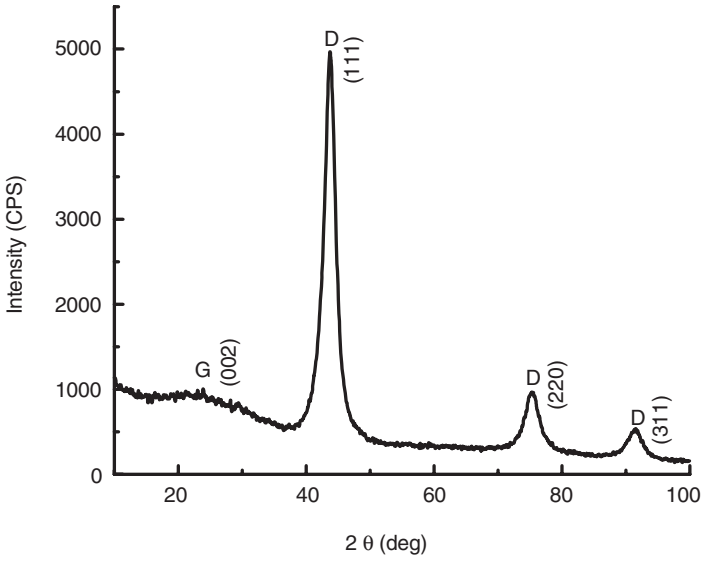

Figure 3. XRD spectrum of the nanodiamond.

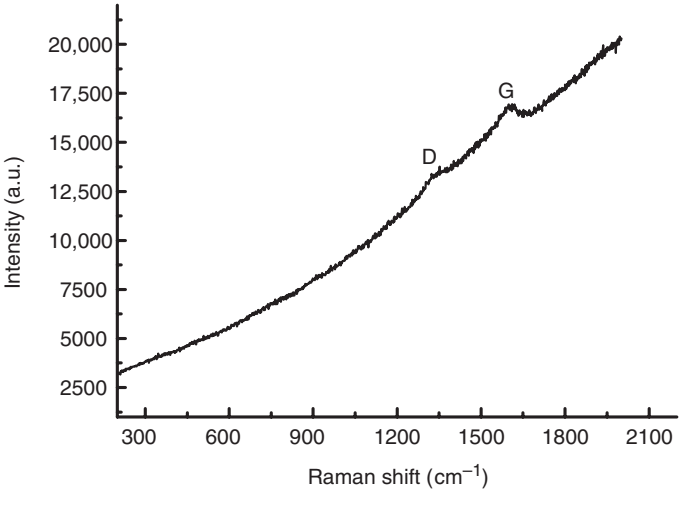

Figure 4. Raman spectrum of the nanodiamond.

at 1616 cm^{-1} was the H_2O bending vibration, which suggested that the surface of the nanodiamond particles had adsorbed a large amount of moisture in the air. The peak at 2920 cm^{-1} was the $-CH_3$ and $-CH_2$ stretching vibration. The peak at 1337 cm^{-1} was caused by –C=O absorption vibration. The peak at 2361 cm^{-1} was due to the absorption vibration of the CO_2.

Figure 6 shows the DSC and thermogravimetric (TG) curve of heating the nanodiamond to 800°C in the air. From the DSC curve shown in Figure 6, we can

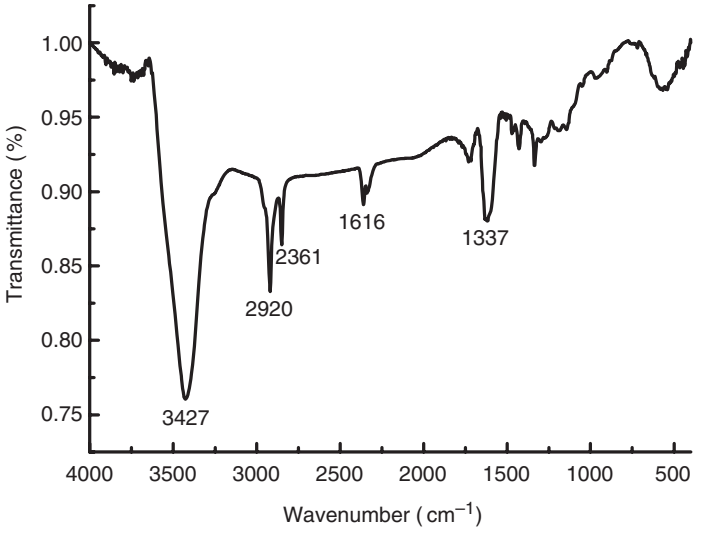

Figure 5. FTIR spectrum of the nanodiamond.

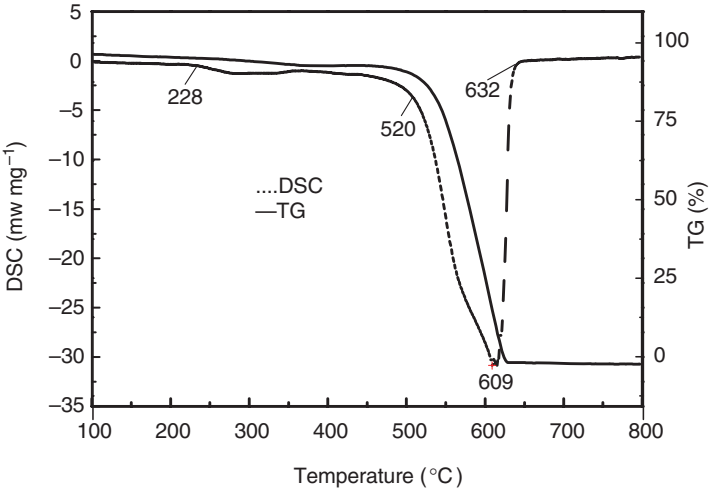

Figure 6. DSC spectrum of the nanodiamond in air.

see that the nanographite existing in the nanodiamond began to be oxidised at the temperature of about 228°C. Afterwards, the nanodiamond began to be oxidised at the temperature of about 520°C. The initial oxidation temperature of the nanodiamond in the air was lower than that of bulk diamond (800°C) due to the smaller size of the nanodiamond particles and larger surface and the nonintegrity of the crystal structure. At the temperature of 632°C, all the nanodiamonds were oxidised completely. Furthermore, the largest heat release peak appeared at the temperature of 609°C. From the TG curve shown in Figure 6, we can see that the weightlessness was almost

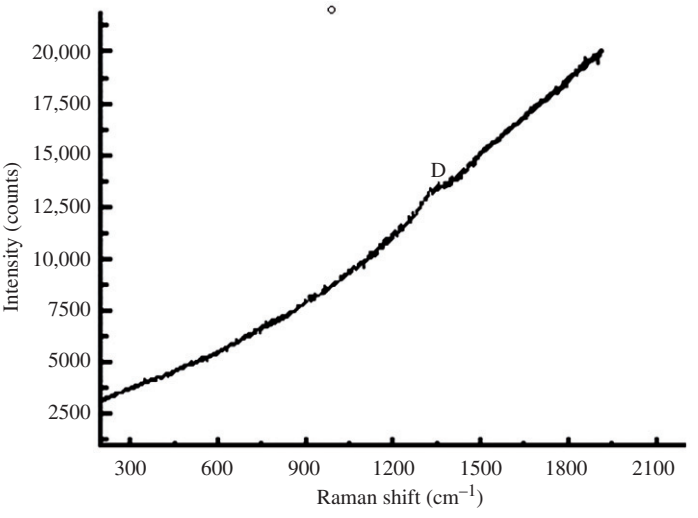

Figure 7. Raman spectrum of the nanodiamond heated up to 350°C in air.

100% at the temperature of 632°C, which also suggested that all the nanodiamonds were oxidised at that temperature.

Figure 7 shows the Raman spectrum of the nanodiamond heated up to 350°C in the air. Comparing to the Raman spectrum shown in Figure 4, we can see that the Raman peak at the vicinity of 1580 cm^{-1}, corresponding to the sp^2 structural nanographite disappeared. However, the Raman peak at the vicinity of 1329 cm^{-1} corresponding to the sp^3 structural nanodiamond still existed. This demonstrated that the sp^2 structural nanographite was oxidised completely after heating the nanodiamond up to 350°C in the air. These results proved that the oxidisation temperature of nanographite was approximately 228°C as shown in Figure 6.

Figure 8 shows the DSC and TG curves of heating the nanodiamond to 1600°C in Ar gas. The TG curve shows obviously that the weightlessness increased with the increase in heating temperature. At the temperature of 1600°C, the weightlessness reached 16%. At the beginning, the weightlessness was mainly due to desorption of some physical functional groups, such as water and CO_2. The peak at the temperature of 406°C was due to desorption of H_2O and CO_2. Following, the weightlessness was mainly due to desorption of some chemical functional groups including –C=O, and so on. The peak at the temperature of 855°C was due to desorption of –C=O, etc. The largest peak at the temperature of 1305°C was due to the transformation of nanodiamond into nanographite at that temperature.

As the nanodiamond is an ultrafine powder, it can be suggested that the major transience caused by the stress during the explosion has been released. Only a small amount of plastic deformation and residual strain were retained in the grains. Therefore, the small nanograin size is the main reason for the diffraction line broadening. If all the line broadening is attributed to the effect of the small grain size, according to the Scherrer formula, the length of the grain in the direction of ⟨111⟩ can be calculated as 3.8 nm.

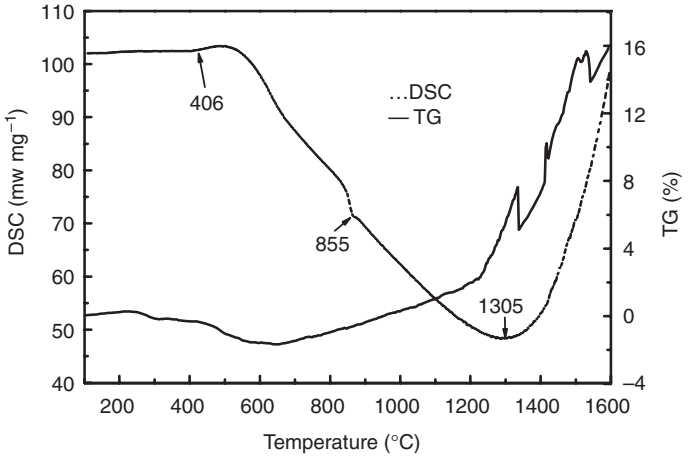

Figure 8. DSC spectrum of the nanodiamond in Ar.

The XRD analysis has identified the lattice constant of the cubic structure nanodiamond as 3.5923 Å. This shows that the lattice constant of the nanodiamond particles synthesised by detonation increases by 0.72% than that of bulk diamonds synthesised by static pressure (the lattice constant of bulk diamond is 3.5667 Å). This may be due to the high-density defects, a mixture of impurity atoms and the lines departing from the position of the balance in the nanodiamond structures.

The size of the nanodiamond observed from the HRTEM image is about 30% different from the grain size calculated with Scherrer equation. X-ray diffraction line width is the best way of measuring grain size. As for the single-crystal particles, the method measures particle size. As for the polycrystalline particles, the law measures the average grain size of a single grain particle composing a single polycrystalline particle. The electron microscope method measures the particle size, rather than grain size; the particle size is the number of average size. It is the most common and most intuitive means of detection of nanoparticle size and distribution. Its result, accurate measurement or not, depends directly on the dispersion of particles. Under normal circumstances, it is a measurement of the diffraction image diameter of a number of grains. If the particles disperse very well, they can become a single grain, HRTEM receives the diffraction image of a single grain. Then the measurement is the diameter of grain, that grain size; it also can observe the morphologies of nanoparticles and even microstructure. In this research, the micro defects, such as twins and stacking faults in a nanocrystal diamond were observed by HRTEM.

The wide Raman peak in the vicinity of 1350 cm^{-1} is the sp^3 structural nanodiamond characteristic peak. The Raman peak observed in the vicinity of 1580 cm^{-1} is the sp^2 structural nanographite. The Raman scattering cross-section of the nanodiamond is 1/30 of the nanographite, which indicates that there is still a small amount of sp^2 structural nanographite residue in the nanodiamond [21]. This result agrees with the XRD results that in the vicinity of $2\theta = 20°–30°$, there is a small peak corresponding to the graphite (0 0 2) surface.

The TNT detonator is a negative oxygen balance explosive used in the experiment for fabricating nanodiamond. Its molecular formula is $C_7H_5N_3O_6$. In the process of reaction,

first, the TNT explosive is decomposed and C, H, O and N atoms are generated. Followed by H, O atoms combine to form H_2O. As the O atoms lessen, only some of the C and O atoms combine to produce CO and CO_2. However, some free C atoms exist in atomic groups. The N atoms combine with each other and produce N_2. During the process of detonator explosion, the initial explosion pressure of the product up to 20–30 GPa and the temperature can be as high as 3000–3500 K. The free carbon atoms or atomic groups generated by TNT diffuse in the reaction area and collide into the nanodiamond, but during the process of explosion, due to the great pressure from the explosion, it is more difficult for the growth of nuclei. In addition, the high pressure continues for a very short (10^{-6}–10^{-7} s below) period after explosion. Therefore, it is too late for the diamond nuclei to grow into larger grains and can only generate a large number of very small size and incomplete crystal ball diamond nanoparticles. In the course of the explosion, N, H and O atoms exist. On the surface of the nanodiamond particles, dangling bonds exist as the result of the structural defects. The H, O and N atoms are adsorbed to the surfaces of the nanodiamond particles. From the results of experiments, C and H atoms combine, thus in the FTIR spectrum of the nanodiamond, there is $–CH_2$ stretching vibration absorption, as well as the $–CH_3$ stretching vibration absorption, which demonstrates that there is a small number of existence of hydrocarbons. Similarly, when C and O atoms combine, there is –C=O and CO_2 bond on the nanodiamond surface and when H and O atoms combine, H_2O generated will be absorbed on the surfaces of the diamond nanoparticles.

4. Conclusions

Nanodiamond has a cubic structure of diamond. Its shape was spherical or elliptical. The average size of the nanodiamond was approximately 5 nm. The lattice constant of the nanodiamond synthesised by detonation was increased by 0.72% than that of the bulk diamonds due to the high-density defects or a mixture of impurity atoms of carbon atoms in the structure of nanodiamond. The surface of the nanodiamond mainly contained –OH, $–CH_3$, $–CH_2$, CO_2, and –C=O groups and so on. The initial oxidation temperature of the nanodiamond was 240°C in the air, which was lower than that of the bulk diamond (550°C).

References

[1] K. Xu and Q.J. Xue, *A new method for deaggregation of nanodiamond from explosive detonation: Graphitization–oxidation method*, Phys. Solid State 46 (2004), pp. 633–634.

[2] A.I. Lyamkin, E.A. Petty, A.P. Ershov, G.V. Sakovich, A.M. Staver, and A.M. Titov, *Ultrafine diamond powders made by the use of explosion energy*, Dokl. Akad. Nauk. SSR. 302 (1988), pp. 611–613.

[3] K. Yamada and A.B. Sawaoka, *Very small spherical crystals of distorted diamond found in a detonation product of explosive/graphite mixtures and their formation mechanism*, Carbon 32 (1994), pp. 665–673.

[4] S. Veprek, *Electronic and mechanical properties of nanocrystalline composites when approaching molecular size*, Thin Solid Films 297 (1997), pp. 145–153.

[5] E. Mironov, A. Koretz, and E. Petrov, *The research of detonation nanodiamond structure by optical methods*, Diamond Relat. Mater. 11 (2002), pp. 872–876.

[6] T. Fujimura, V.Y. Dolmatov, G.K. Burkat, E.A. Orlova, and M.V. Veretennikova, *Electrochemical codeposition of Sn-Pb-metal alloy along with detonation synthesis nanodiamonds*, Diamond Relat. Mater. 13 (2004), pp. 2226–2229.
[7] G.K. Burkat, T. Fujimura, V.Y. Dolmatov, E.A. Orlova, and M.V. Veretennikova, *Preparation of composite electrochemical nickel–diamond and iron–diamond coatings in the presence of detonation synthesis nanodiamonds*, Diamond Relat. Mater. 14 (2005), pp. 1761–1764.
[8] N.I. Chkhalo, M.V. Fedorchenko, E.P. Krulyako, A.I. Volokhov, and K.S. Baraboshkin, *Ultradispersed diamond powders of detonation nature for polishing X-ray mirrors*, Nucl. Instrum. Methods Phys. Res. Sect. A. 359 (1995), pp. 155–156.
[9] N.I. Chkhalo, M.V. Fedorchenko, E.P. Kruglyakov, A.I. Volokhov, K.S. Baraboshkin, V.F. Komarov, S.I. Kostyukov, and E.A. Petrov, *Ultradispersed diamond powders of detonation nature for polishing X-ray mirrors*, Nucl. Instrum. Methods A 359 (1995), pp. 155–156.
[10] L.N. Tsai, G.R. Shen, Y.T. Cheng, and W. Hsu, *Performance improvement of an electrothermal microactuator fabricated using Ni-diamond nanocomposite*, J. Microelectromech. Syst. 15 (2006), pp. 149–158.
[11] R.J. Narayan, *Pulsed laser deposition of functionally gradient diamond-like carbon-metal nanocomposites*, Diamond Relat. Mater. 14 (2005), pp. 1319–1330.
[12] E.A. Ekimov, E.L. Gromnitskaya, S. Gierlotka, W. Lojkowski, B. Palosz, A. Swiderska-Sroda, J.A. Kozubowski, and A.M. Naletov, *Mechanical behavior and microstructure of nanodiamond-based composite materials*, J. Mater. Sci. Lett. 21 (2002), pp. 1699–1702.
[13] N. Kossovsky, A. Gelman, and H.J. Hnatyzyn, *Surface-modified diamond nanoparticles as antigen delivery vehicles*, Bioconjugate Chem. 6 (1995), pp. 507–511.
[14] I.B. Yanchuk, M.Y. Valakh, A.Y. Vul', V.G. Golubev, S.A. Grudinkin, and N.A. Feoktistov, *Raman scattering, AFM and nanoindentation characterisation of diamond films obtained by hot filament CVD*, Diamond Relat. Mater. 13 (2004), pp. 266–269.
[15] A. Hiraki, *Low-temperature (200°C) growth of diamond on nano-seeded substrates*, Appl. Surf. Sci. 162–163 (2000), pp. 326–331.
[16] N.R. Greiner, D.S. Phillips, J.D. Johnson, and F. Volk, *Diamonds in detonation soot*, Nature 333 (1988), pp. 440–442.
[17] V.M. Titov, V.F. Anisichkin, and I.Y. Mal'kov, *Investigation of the ultra-dispersed diamond*, Fizika Goreniya I Vzryva 25 (1989), pp. 117–126.
[18] A.I. Lyamkin, E.A. Petrov, A.P. Ershov, G.V. Sakovich, and A.M. Staver, *Production of diamond from explosives* (in Russian), Sov. Phys. Dokl. 33 (1988), pp. 705–706.
[19] A.E. Alexensky, M.V. Baidakova, A.Y. Vul', V.Y. Davydov, and Y.A. Pevtsova, *Diamond–graphite phase transition in clusters of ultrafine diamond*, Phys. Solid State 39 (1997), pp. 1007–1015.
[20] M.V. Baidakova, A.Y. Vul', V.I. Siklitskii, and N.N. Faleev, *Fractal structure of ultradisperse-diamond clusters*, Phys. Solid State 40 (1998), pp. 715–718.
[21] P.W. Chen, Y.S. Ding, Q. Chen, F.L. Huang, and S.R. Yun, *Spherical nanometer-sized diamond obtained from detonation*, Diamond Relat. Mater. 9 (2000), pp. 1722–1725.